THE UNIVERSITY of EDINBURGH

Edinburgh Research Explorer

Recovery of phosphate from municipal wastewater as calcium phosphate and its subsequent application for the treatment of acid mine drainage

Citation for published version:
Nepfumbada, C, Tawanda Tavengwa, N, Masindi, V, Foteinis, S & Chatzisymeon, E 2023, 'Recovery of phosphate from municipal wastewater as calcium phosphate and its subsequent application for the treatment of acid mine drainage', *Resources, Conservation and Recycling*, vol. 190, 106779. https://doi.org/10.1016/j.resconrec.2022.106779

Digital Object Identifier (DOI):
10.1016/j.resconrec.2022.106779

Link:
Link to publication record in Edinburgh Research Explorer

Document Version:
Peer reviewed version

Published In:
Resources, Conservation and Recycling

General rights
Copyright for the publications made accessible via the Edinburgh Research Explorer is retained by the author(s) and / or other copyright owners and it is a condition of accessing these publications that users recognise and abide by the legal requirements associated with these rights.

Take down policy
The University of Edinburgh has made every reasonable effort to ensure that Edinburgh Research Explorer content complies with UK legislation. If you believe that the public display of this file breaches copyright please contact openaccess@ed.ac.uk providing details, and we will remove access to the work immediately and investigate your claim.

Download date: 19. Feb. 2023

Recovery of phosphate from municipal wastewater as calcium phosphate and its subsequent application for the treatment of acid mine drainage

Collen Nepfumbada[1], Nikita Tawanda Tavengwa[1], Vhahangwele Masindi[2&3], Spyros Foteinis[4], Efthalia Chatzisymeon[5].

[1]Department of Chemistry, School of Mathematics and Natural Sciences, University of Venda, Private Bag X5050, Thohoyandou, 0950, South Africa.

[2]Magalies Water (MW), Scientific Services (SS), Research & Development (R&D) Division, Erf 3475, Stoffberg street, Brits, 0250, South Africa, tel: 0123816602.

[3]Department of Environmental Sciences, College of Agriculture and Environmental Sciences, University of South Africa (UNISA), P.O. Box 392, Florida,1710, South Africa.

[4]Research Centre for Carbon Solutions, School of Engineering and Physical Sciences, Heriot-Watt University, Edinburgh EH14 4AS, United Kingdom.

[5]School of Engineering, Institute for Infrastructure and Environment, University of Edinburgh, Edinburgh EH9 3JL, United Kingdom

Abstract

Here, the co-treatment of municipal wastewater (MWW) and acid mine drainage (AMD) is proposed, where the recovered low-value phosphorus from MWW is used for the treatment of AMD. Specifically, MWW was treated using calcium hydroxide ($Ca(OH)_2$), a low-cost and readily available material, with the ammonia content being greatly reduced (89%) through stripping and phosphates practically eliminated (>99%). The recovered low-value phosphorus material, in the form of calcium phosphate ($Ca_3(PO_4)_2$), was then used for the treatment of AMD from coal mining. Metals contained in AMD scavenged phosphorous, forming new

minerals, and the increased alkalinity led to their precipitation. The optimum treatment conditions were 90 min contact time, 10 g L^{-1} $Ca_3(PO_4)_2$ dosage, and room temperature and ambient pH. Under these conditions, AMD's metal content (Fe, Mn, Cr, Cu, Ni, Pb, Al, and Zn) was practically depleted (>99% removal) and sulphate (SO_4) greatly reduced (90.6%). Results were underpinned by FTIR, FIB/SEM, EDS/SEM, XRF, and XRD.Overall, this indirect co-treatment method holds great promise for the sustainable management of both wastewater matrices and can provide a simple and effective solution for their co-management, particularly in the developing world context where it could also help in advancing the UN's sustainable development goals.

Keywords: Acid and metalliferous drainage (AMD) or acid rock drainage (ARD); sustainable wastewater management; water reclamation; wastewater valorisation; minerals synthesis and recovery; zero liquid discharge (ZLD) and circular economy.

1 Introduction

The increasing contamination of terrestrial and aquatic ecosystems by acid mine drainage (AMD) and municipal wastewater (MWW) effluents has been an issue of emerging environmental concern, both at national and international level, and particularly in low and middle income countries (LMIC), since these pose numerous ecological stresses (The United Nations, 2018). These stresses are grossly traced back to the release of untreated or poorly treated AMD and/or MWW to different receiving environments and this problem has exacerbate during the past decades. The problem persists in countries with strong mining industry and rapid population growth, such as South Africa. In particular, AMD comprise elevated levels of inorganic contaminants, including (heavy)-metals (e.g., Al, Fe, Cu, Mn, Ni, and Zn), metalloids, oxyanions, radionuclides, and rare earth elements, along with high acidity

in the form of hydrogen ions (Simate and Ndlovu, 2014, Kefeni et al., 2017, Park et al., 2019). Its physicochemical properties greatly vary, depending on the host geology being weathered. For example, the oxidation of pyrite (FeS_2) or other sulfide (S^{2-}) bearing minerals, which is typically catalysed by certain bacteria communities, will result in AMD rich in iron (Fe) and sulphate (SO_4^{2-}) (Baker and Banfield, 2003, Sheoran et al., 2011, Wei et al., 2016, Masindi et al., 2022c).

On the contrary, MWW comprise elevated levels of chemical oxygen demand (COD), phosphate (PO_4^{3-}), ammonia (NH_3), and base metals, as well as microbiological contaminants, which can all cause great harm to the environment if released untread (Petrie et al., 2015, Arola et al., 2019, Mavhungu et al., 2020). Even though MWW contains phosphorus (P), its recovery in small to medium facilities can be problematic due to its low concentration which results in a P-product with limited commercial value, unless if a coupling technology is integrated to enhance the grade of the recovered phosphate mineral (Bunce et al., 2018). As such, the low-value P sludge that is generated during MWW treatment has little to no economic value, especially when recovery is pursued without P pre-concentration (Masindi and Foteinis, 2021).

Therefore, contaminants contained in both streams are of major concern to the receiving environment. For example, metals embodied in AMD pose adverse eco-toxicological effects upon exposure (Kefeni et al., 2017), whereas nutrients contained in MWW are notorious for the eutrophication pressures on inland waters (Bouwer, 2000, Soucek et al., 2000, Amann et al., 2018). As a result, these effluents should be preferably treated before being discharged into the environment. However, in LMICs only 8% - 38% of the municipal and industrial wastewater is currently been treated (United Nations., 2017), highlighting the need for large scale treatment initiatives in these settings.

A wide array of technologies have been proposed and developed for the treatment of these effluents. Specifically, for the treatment of AMD active and passive technologies are typically employed, with the first being more efficient in contaminants removal, since alkaline materials such as lime, magnesite, periclase, brucite, or soda ash, are used, but at the expense of cost and complexity (Kefeni et al., 2017, Masindi et al., 2018c, Naidu et al., 2019, Neculita and Rosa, 2019, Park et al., 2019). On the other hand, biological process are often employed in MWW treatment (Oehmen et al., 2007, Zhao et al., 2014), nonetheless, in LMIC, MWW is often released untreated or poorly treated, greatly affecting local communities and receiving ecosystems (UN Habitat and WHO, 2021). However, one the of MWW's main contaminants, i.e., P, presents certain advantages for AMD treatment since AMD's metal content will scavenge P leading to minerals formation which can then be more easily precipitated and removed (Masindi et al., 2022b). In this regard, hydrated lime ($Ca(OH)_2$) can be used for P recovery from MWW, since the released calcium (Ca) from the $Ca(OH)_2$ matrix will react with P and lead to the synthesis and precipitation (due to alkalinity increase) of calcium phosphate ($Ca_3(PO_4)_2$) (Tong et al., 2021).

Therefore, research has also focused on the effective co-treatment of both effluents (Strosnider et al., 2011a, Hughes and Gray, 2013a), mainly by examining passive co-treatment (Strosnider et al., 2011b), direct mixing without the addition of chemical reagents (Spellman et al., 2020, Masindi et al., 2022b), and the use of MWW activated sludge for AMD treatment (Hughes and Gray, 2013b, Barthen et al., 2022). Furthermore, focus has also been placed on the removal of P from MWW, when using raw AMD (co-treatment) (Ruihua et al., 2011), AMD flocs (Adler and Sibrell, 2003, Sekhon and Bhumbla, 2013), or AMD sludge (Wei et al., 2008, Yulianto et al., 2021). The use of struvite, also known as magnesium ammonium phosphate (MAP), that has been synthesized from MWW (Petrie et al., 2015, Arola et al., 2019, Mavhungu et al.,

2020), has also been proposed for AMD treatment (Masindi et al., 2022a). However, the use of $Ca_3(PO_4)_2$, which is simpler to be synthesized and recovered from MWW (Masindi and Foteinis, 2021) than struvite (Mavhungu et al., 2020b), for AMD treatment has not yet been covered by the existing body of knowledge and remains an important research gap. This indirect co-treatment method can hold great promise, particularly for LMICs where wastewater tend to be released untreated or partially treated (United Nations., 2017). Furthermore, it can help advancing the UN's sustainable development goals (SDGs) (The United Nations, 2018), since not only the receiving environment will be protected but water could also be reclaimed and used for different purposes, ranging from irrigation, groundwater recharge, or even for drinking water. Here, this research gap is filled by synthesizing $Ca_3(PO_4)_2$ from P-rich MWW (i.e., effluent collected from a sludge dewatering stream within a MWW treatment plant) and then employing it for the treatment of AMD from coal mining.

2 Materials and methods

2.1 Wastewater samples collection

The MWW that was used herein was collected from the dewatering stream, i.e., filter press, of a MWW treatment facility in Tshwane Metropolitan Municipality, Pretoria, South Africa. As such, the effluent was rich in PO_4^{3-} and NH_3, among others (**Table 1**), and therefore can be categorised as high-strength MWW (Qteishat et al., 2011, Rahman et al., 2020). For example, MWW with phosphorus concertation higher than 20 mg L^{-1} and nitrogen higher than 85 mg L^{-1} can be regarded as strong (Qteishat et al., 2011), whereas here the ammonia and phosphate concentrations of the collected MWW were higher than 120 and 180 mg L^{-1}, respectively (**Table 1**). It should be noted that the treatment facility daily receives around 65 megaliters (ML) of wastewater, emanating from a number of activities from the surrounding area.

Furthermore, the AMD was collected from a coal mine in Mpumalanga province, South Africa. The effluent was seeping through the toe of a coal stockpile into a small evaporation pond, and as such it can be also considered as high-strength (Strosnider and Nairn, 2010). For effluent (AMD and MWW) collection, wide-mouth high-density polyethylene (HDPE) bottles were used. Furthermore, similar to the pre-treatment process in conventional treatment facilities, to ensure that suspended solids and debris will not impose on the treatment process, the collected effluents (AMD and MWW) were passed through Macherey-Nagel filter papers (MN 615. Ø125mm). After collection, samples were stored in a cooled bag and transferred to the laboratory

2.2 Calcium phosphate synthesis

For synthesis of $Ca_3(PO_4)_2$ from the collected MWW $Ca(OH)_2$ was used, which was procured, in 25 kg fabric bags, from Protea Chemicals, (Pty) Ltd. The optimal $Ca(OH)_2$ dosage and contact time for $Ca_3(PO_4)_2$ synthesis from MWW have been reported by Weaver and Ritchie (1994) and Dunets and Zheng (2014), and further verified by Masindi and Foteinis (2021). Specifically, a solid ($Ca(OH)_2$) to liquid (MWW) (S:L) ratio of 1 g : 100 mL was considered, while the mixing duration (i.e., contact time) was 60 min. After mixing, 30 min of equilibrium time was considered, as to ensure that the crystallized sludge was fully settled. The supernatant was moved to another beaker, and the $Ca_3(PO_4)_2$ sludge was collected and dried (at 105 ℃ for 24 hours), before being pulverised, using a ball miller, and passed through a 100 µm perforated sieve to obtain a fine particle size and homogenised material (Masindi and Foteinis, 2021).

2.3 Experimental setup for AMD treatment and optimisation studies

All experiments were performed at bench scale, using volumetric flasks filled with 1,000 mL of AMD. To enable the $Ca_3(PO_4)_2$ to effectively come into contact with the contaminants

contained in AMD an overhead stirrer was employed, which was set at 250 rpm. In real-world applications, and particularly in LMICs, this treatment process is expected not only to be cost-effective, but also to be simple to scale up and operate. As such, the temperature and the pH during AMD treatment were not controlled, i.e., their ambient values were considered.

Therefore, the parameters that were considered in the optimisation studies include the: i) contact time (i.e., mixing duration of $Ca_3(PO_4)_2$ with the AMD), and ii) $Ca_3(PO_4)_2$ dosage (i.e., the $Ca_3(PO_4)_2$ mass per AMD volume (S:L ratio)). The effect of these two main parameters on AMD treatment efficiency was examined by first varying the contact time and then the $Ca_3(PO_4)_2$ dosage. Therefore, the optimum contact time was first identified, examining the following mixing durations: 5, 10, 15, 30, 45, 60, 90, and 180 min. Then, the optimum contact time was used to identify the optimum $Ca_3(PO_4)_2$ dosage, examining the following dosages: 0.5, 1, 2.5, 5, 10, 15, and 25 g. The $Ca_3(PO_4)_2$ mass was measured using an analytical balance, with the precision being restricted to 2-decimal places. Finally, all experiments were performed in triplicate and results are presented as mean values. Results were deemed acceptable if, statistically, they were within the 95% confidence interval.

2.4 Sample characterization

To identify the chemical species contained in the examined aqueous matrices (AMD and MWW, before and after treatment with $Ca(OH)_2$ and $Ca_3(PO_4)_2$ respectively), as well as to identify the purity of the procured $Ca(OH)_2$ and the composition of the synthesized $Ca_3(PO_4)_2$ and of the sludge that is generated from the interaction of $Ca_3(PO_4)_2$ with the AMD (resultant sludge thereafter), different analytical techniques were employed. Specifically, experiments were carried out in the ISO/IEC 17025:2017 accredited laboratory of Magalies Water Services,

161 in Brits, North West, South Africa using different analytical pieces of equipment as discussed
162 below.

163 **2.4.1 Aqueous samples characterization**

164 The pH and specific conductance (electrical conductivity at 25 °C) of both examined aqueous
165 samples (MWW and AMD), before and after treatment, were measured by means of a multi-
166 parameter probe (HANNA instrument, HI9828). The chemical species contained in the raw
167 effluents were measured by means of inductively coupled plasma - optical emission
168 spectroscopy (ICP-OES) (Agilent Technologies 5110, coupled with Agilent SPS 4 Auto
169 sampler) while the chemical species contained in the treated effluents were measured by means
170 of inductively coupled plasma mass spectrometry (ICP-MS) (Thermo Scientific's XSERIES 2,
171 coupled with ASX-520 auto sampler). Thermo Fisher Scientific gallery plus discrete analyser
172 photo spectrometer was used for base metals analyses, including sulphates. The total plate
173 count (TPC) was determined following the American Public Health Association (APHA)
174 guidelines. Specifically, a defined volume of the sample was transferred into a 90 mm size Petri
175 dish, along with molten agar, and mixed thoroughly. After solidification, the agar plates were
176 inverted and incubated at 36˚C for 48 hours (Greenberg et al., 2010). After incubation, the
177 colonies were observed to arise from single cells, pairs, chains, to clusters, all of which were
178 included in the colony forming units. Similar to TPC, the total coliform and *E. coli*
179 concentrations were measured following the APHA guidelines. Specifically, the membrane
180 filtration technique was used, where the sample is passed through a cellulose filter (0.45 µm
181 pore size) and then the filter is placed on agar mediums and incubated at 36˚C for 24 hours,
182 before measuring the bacteria concentrations (Greenberg et al., 2010). The aforementioned
183 pieces of equipment were utilised interchangeably, depending on availability and

characterization needs. Finally, National Institute of Standards and Technology (NIST) reference materials and quality control procedures were duly considered during the experiments and analyses.

2.4.2 Solid samples characterization

To ascertain the mineralogical characteristics of the: i) procured $Ca(OH)_2$, ii) synthesized $Ca_3(PO_4)_2$ (from the interaction of $Ca(OH)_2$ with MWW), and iii) resultant sludge (from the interaction of $Ca_3(PO_4)_2$ with AMD), X-ray diffraction (XRD) (Panalytical X'Pert PRO X-ray diffractometer along with Philips PW 1710 Diffractometer with graphite secondary monochromatic source) was used. Furthermore, their elemental compositions were ascertained using X-ray fluorescence (XRF) (Thermo Scientific ARL PERFORM'X Sequential X sequential XRF spectrometer, coupled with the UniQuant software for standardless quantitative analysis), while the metals and anions functional groups were ascertained using Fourier transform infrared spectroscopy (FTIR), making use of Perkin-Elmer Spectrum 100 FTIR spectrometer coupled with Perkin-Elmer's universal attenuated total reflectance (ATR) sampling accessory with a diamond crystal. To corroborate and complement the XRD and XRF results, the morphological, mapping, and elemental properties were ascertained using high resolution (HR) field emission scanning electron microscope (FE-SEM) (SmartSEM®-Auriga®) coupled with focused ion Beam (FIB) and energy dispersive X-ray spectroscopy (EDS).

3 Results and discussions

3.1 Calcium phosphate synthesis from municipal wastewater

The interaction of $Ca(OH)_2$ with the high-strength MWW, i.e., the P-rich effluent from the sludge dewatering stream, does not only lead to the synthesis of $Ca_3(PO_4)_2$ but also to a large reduction in MWW's main contaminants, including biological contaminants, as shown in **Table 1**. The optimal conditions for $Ca_3(PO_4)_2$ synthesis from MWW are discussed elsewhere (Masindi and Foteinis, 2021) and include ambient temperature and pH, i.e., room temperature and 7.8 pH, 60 min contact time (stirring at 250 rpm) and an S:L ($Ca(OH)_2$:MWW) ratio of 10 g per L (w/v). This will lead to a large increase of the pH of the wastewater, leading to the removal of different contaminants, as will be discussed below, while the generated supernatant will also have a high pH value (≥11.5) as shown in **Table 1**.

Table 1: The chemical composition of the high-strength MWW (effluent from the sludge dewatering stream), before and after the $Ca_3(PO_4)_2$ synthesis.

Parameter	**Units**	**Before treatment**	**After treatment**
pH	-	7.8	11.5
Ammonia	mg L^{-1} (ppm)	180	20
Phosphate	mg L^{-1}	120	0.1
Ca	mg L^{-1}	27	135
Mg	mg L^{-1}	30	0.05
E. coli	counts 100 mL^{-1}	≥241960	ND
Total coliforms	MPN/100 ml	≥2420	ND
Total plate counts	count/1mL	≥29500	2

Specifically, phosphates were practically removed (≥99.9%) while ammonia can be greatly removed, but only after sufficient residence time (24 hrs). It was identified that after 30 min of residence time, which is required for the precipitation of the synthesized $Ca_3(PO_4)_2$, ammonia

is reduced by 42% (Masindi and Foteinis, 2021). However, if longer residence times (≥4 hours) were to be employed, then ammonia reduction greatly improves (88% reduction, Table 2). The large reduction in ammonia content is most likely traced based to stripping, following Le Chatelier's principle of equilibrium. In this case, the high pH (≥11.5) of the treated effluent in combination with the relatively high temperature (room temperature in South Africa can be as high as 26^{o}C) could be the main reasons for high ammonia reduction, in addition to high residence time (O'Farrell et al., 1972, Kim et al., 2021). High reduction in the ammonia content through stripping is common and has been widely reported in literature. For example, Calli et al. (2005) explored the removal of ammonia from landfill leachates, through air stripping and at pH 11 and 20 ^{o}C, and a steep increase in the percentage removal was observed with increasing residence time (~70% and ~94% of ammonia was striped after 4 and 12 h respectively), hence corroborating findings in this study.

It should be noted that here high-strength MWW, i.e., effluent from a sludge dewatering stream, was used instead of weak- or medium-strength MWW (Qteishat et al., 2011, Rahman et al., 2020). The reason is that for phosphorus recovery applications effluents rich in phosphorous, i.e., high-strength MWW, are typically preferred (Masindi and Foteinis, 2021). Medium- or even weak-strength MWW could be used to produce $Ca_3(PO_4)_2$, however, most likely, higher MWW quantities would be required due to the lower phosphorous concentration. Nonetheless, the medium- or weak- strength MWW would also enjoy a high degree of treatment, as is the case with the high-strength MWW, highlighting the potential of incorporating the proposed process in existing or new MWW facilities. On the other hand, phosphates were adsorbed by the Ca, which was released from $Ca(OH)_2$ into the MWW matrix and towards the synthesis of $Ca_3(PO_4)_2$. Under the examined conditions, $Ca(OH)_2$ was able to fully absorb (≥99.9%) MWW's P content. The equations governing P scavenging and

precipitation as $Ca_3(PO_4)_2$ can be found elsewhere (Masindi and Foteinis, 2021). Regarding Mg, its levels were similarly depleted (≥99.9% reduction). This suggests that Mg co-precipitates in the $Ca_3(PO_4)_2$ matrix, as this has also been highlighted elsewhere (Vo et al., 2022).

Henceforth, the Ca levels of the treated MWW were observed to have been increased significantly. As mentioned above, Ca is released during $Ca(OH)_2$ dissolution and therefore its increased dissolution, at least until the mixture becomes supersaturated with respect to Ca, is responsible for the elevated Ca levels in the treated effluent (**Table 1**). Furthermore, $Ca(OH)_2$ is responsible for the elevated pH levels, i.e., from pH ≥7.8 in raw MWW to ≥11.5 in the treated effluent. This high pH levels suggests that the treated effluent cannot be directly released to the environment, however it also has certain advantages. First, the high pH leads to the removal of biological contaminants (**Table 1**). Specifically, when using caustic solutions such as $Ca(OH)_2$, alkaline disinfection can be achieved. The reason is that at pH ≥9 and above the free hydroxyl ions (OH^-) will exert antimicrobial activity and inhibit most bacteria and many viruses (mainly the non-enveloped ones) since OH^- can damage the bacterial cytoplasmic membrane, denature enzymes and structural proteins, and also damage the DNA (Tilbury et al., 2017). Furthermore, the high Ca, and by extension pH levels, can be beneficial for other uses, since, for example, through bubbling the treated effluent can be used to possibly uptake CO_2 (an acidic gas) from point sources such as fossil fuel power stations or even from the atmosphere (a much slower process) until equilibrium. Finally, if AMD is in close proximity, the treated effluent can be used for the neutralisation or even possibly for the treatment of raw AMD (Masindi et al., 2022d), which highlights the potential many uses of the treated effluent.

3.2 Optimisation studies

To evaluate the effect of contact time and $Ca_3(PO_4)_2$ dosage a wide range of values, for each parameter, was examined, and results are discussed below.

3.2.1 Effect of contact time

The variations in EC, pH, Ca, and Mg levels with increasing contact time are shown in **Figure 1**.

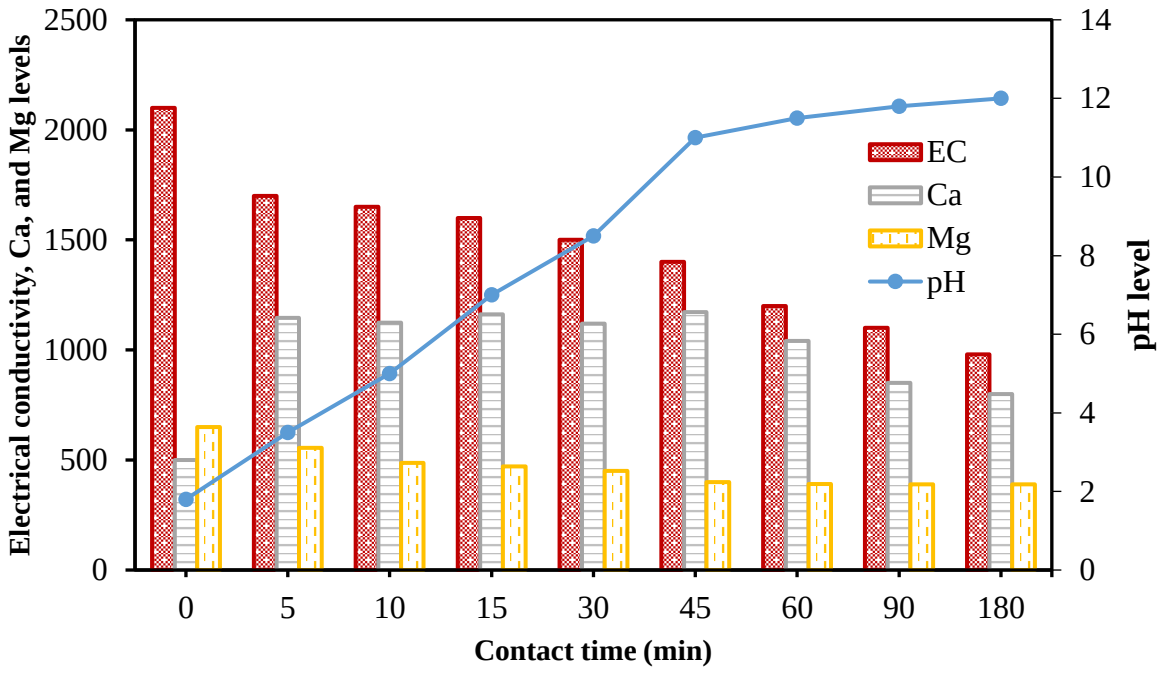

Figure 1: Variation in electrical conductivity (EC) (mS/cm), pH, Ca (mg L^{-1}), and Mg (mg L^{-1}) levels with increasing contact time (range 5 - 180 min) during the treatment of acid mine drainage (AMD) with $Ca_3(PO_4)_2$ (dosage 10 g per 1000 mL, 250 rpm mixing speed, and room temperature).

Regarding the results shown in **Figure 1**, a decrease in EC denotes the removal of ions from the aqueous solution. This could be linked to the removal of Mg and other metals contained in AMD. Nonetheless, the increased levels of Ca do not allow the EC levels to be greatly reduced,

even at the 180 min contact time. Furthermore, up to 60 minutes of contact time the supernatant's pH was observed to increase with increasing contact time, and thereafter it was observed to stabilize. The increase in pH is traced back to the increased dissolution of $Ca_3(PO_4)_2$ with increasing contact time.

An inverse correlation was observed between Ca and Mg levels in the 5 - 45 min contact time range. Specifically, in this range, Ca concentration was observed to increase with increasing contact time, whereas the Mg levels were decreasing with increasing contact time. However, at 60 - 180 min contact time both the Ca and Mg levels were decreasing with increasing contact time. The increase in Ca levels in the 5 - 45 min range suggest the increase dissolution of $Ca_3(PO_4)_2$ in this range, since AMD might be unsaturated with respect to Ca-carbonates, whereas the decrease after the 60 min contact time might suggest that the solution is (super)saturated with respect Ca-carbonates and that Ca-based minerals could precipitate. Therefore, the contact time should be at least 45 min, where it appears that $Ca_3(PO_4)_2$ reaches its maximum dissolution. However, even after 45 min contact time acidity is still removed, since the pH increases, but at a significantly lower rate compared to contact time 5 - 45 min. On the other hand, the levels of Mg were observed to decrease with increasing contact time, suggesting that Mg is scavenged by $Ca_3(PO_4)_2$ from the lower end of the examined contact time range and precipitates. Regarding the variations in the percentage removal of the main chemical species contained in the AMD, i.e., Fe, Mn, Cr, Cu, Ni, Pb, Al, SO_4, and Zn, with increasing contact times, these are shown in **Figure 2**.

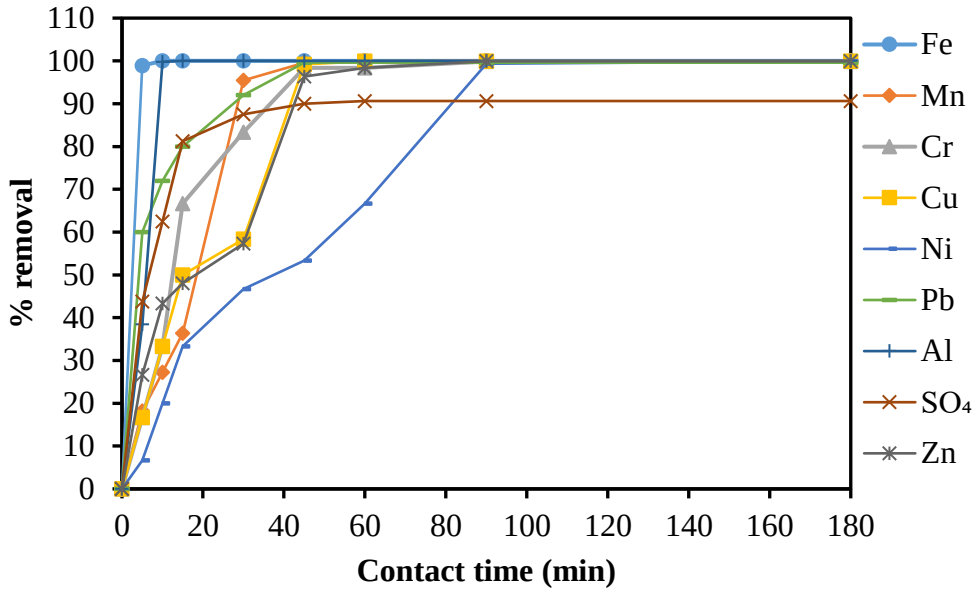

299

300 **Figure 2:** Variations in the percentage removals of the main chemical species contained in
301 AMD with increasing contact times (10 g per 1000 mL, 250 rpm mixing speed, and room
302 temperature).

303 As shown in **Figure 2**, there was a rapid increase in the percentage removal of most examined
304 contaminants, even at the lower values of the examined contact time range, and particularly for
305 Fe, which was practically removed after 5 min contact time, and Pb, which was greatly reduced
306 (60.0%). As the contact time increases, the percentage removals increase as well, with Al being
307 practically removed (≥99.8%) at contact time 10 min. Apart from Ni, the concentrations all
308 other contaminants steeply decreased, i.e., percentage removals increase, with increasing
309 contact times. Specifically, at 45 min these contaminants were greatly depleted (percentage
310 removals 96.3%) while at 60 min were practically removed (percentage removals ≥ 99.6%)
311 apart from Cr which percentage removal is optimized at 80 min, i.e., ≥99.83% instead of 98.3
312 in 60 min. On the other hand, the Ni levels were also reduced with increasing contact time, but
313 at a slower rate compared to the other examined metals, i.e., the percentage removal at 45, 60,

and 90 min was 53.3%, 66.7%, and 99.3% respectively. Similarly, the 90 min contact time appears to also optimize Ni removal. On the other hand, a different pattern was observed for SO_4 removal. Specifically, a steep decrease in the first three examined contact times was observed, since 43.8%, 62.5%, and 81.3% was removed at 5, 10, and 15 min respectively. However, thereafter its percentage removal only gradually increases (87.5% in 45 min) and it appears to reach a plateau at 60 min contact time (90.6% removal). The obtained results are in line with the results of Maree et al. (2013), where AMD treated with ≥12.53 g L^{-1} $Ca(OH)_2$ and for 90 min contact time, lead to an 83% reduction of the SO_4 content, i.e., from 16200 to 2826 mg L^{-1}. This suggest $Ca_3(PO_4)_2$ is more potent than $Ca(OH)_2$ in SO_4 removal from AMD and also brings forward the importance of P in the AMD treatment.

Overall, the removal of contaminants was observed to be dependent on the contact time. The underlying reason is that with increasing contact time, the dissolution of $Ca_3(PO_4)_2$ increases. Therefore, more P and alkalinity are available, with metals such as Fe scavenging the P (Masindi and Foteinis, 2021), while the alkalinity will gradually increase the pH and lead to metals and minerals precipitation (Masindi et al., 2018b). As a result, the use of $Ca_3(PO_4)_2$ for the treatment of AMD combines the benefits of alkalinity increase and metal-P scavenging. Regarding the optimum contact time, 90 min appears to maximize contaminants removal, and particularly the removal of Cr and Ni, but not at the expense of treatment operation (increased mixing duration translates to increased capital and operating costs). The mixing speed might also affect the system, since, most likely, under slower mixing speeds longer contact times might be required. This, and other factors such as the temperature, will be examined in future works of our group. Therefore, 90 min was considered as the optimum time for the removal of different contaminants from the concentrated AMD (**Figure 1** and **2**) and this value was then used in $Ca_3(PO_4)_2$ dosage optimization experiments.

3.2.2 Effect of calcium phosphate dosage

The effect of $Ca_3(PO_4)_2$ dosage was also examined by first studying the variations in EC, pH, Ca, and Mg levels with increasing dosages. Results are shown in **Figure 3**.

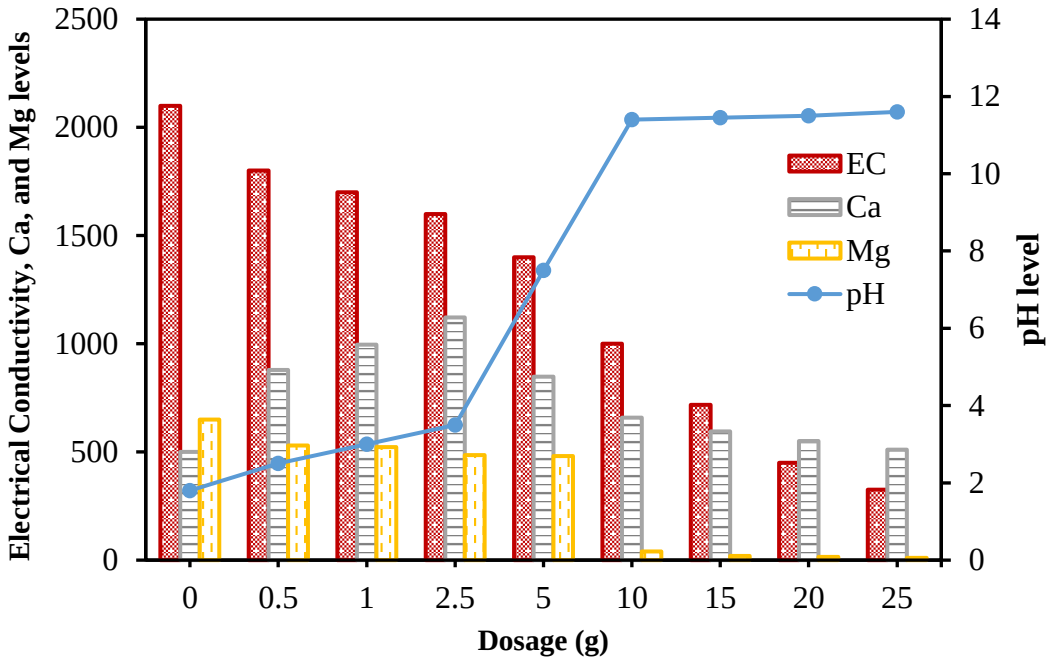

Figure 3: Variation in electrical conductivity (EC) (mS/cm), pH, Ca (mg L^{-1}), and Mg (mg L^{-1}) with increasing $Ca_3(PO_4)_2$ dosages (contact time 90 min, acid mine drainage (AMD) volume 1000 mL, 250 rpm mixing speed, and room temperature).

As shown in **Figure 3**, EC was decreasing with increasing $Ca_3(PO_4)_2$ dosage and this could be attributed to the removal of metals and SO_4 contained in the concentrated AMD (**Table 2**). Specifically, the interaction of Ca, which is released from the $Ca_3(PO_4)_2$ matrix, with AMD's SO_4 content can result to the formation of gypsum (Masindi et al., 2018a, Masindi and Foteinis, 2021) and its subsequent precipitation. Increasing $Ca_3(PO_4)_2$ dosages lead to increasing pH values, since additional alkalinity will be available to the system which promotes the

precipitation of metals and minerals. Finally, regarding the Mg levels, an up to 5 g L^{-1} $Ca_3(PO_4)_2$ dosage will lead to only a small percentage reduction (26%), whereas the 10 g L^{-1} $Ca_3(PO_4)_2$ dosage greatly reduces (93.8%) the Mg level. Thereafter, the Mg concentration appear to remain nearly constant, since a very mild decrease in its levels is observed with increasing dosages (**Figure 3**).

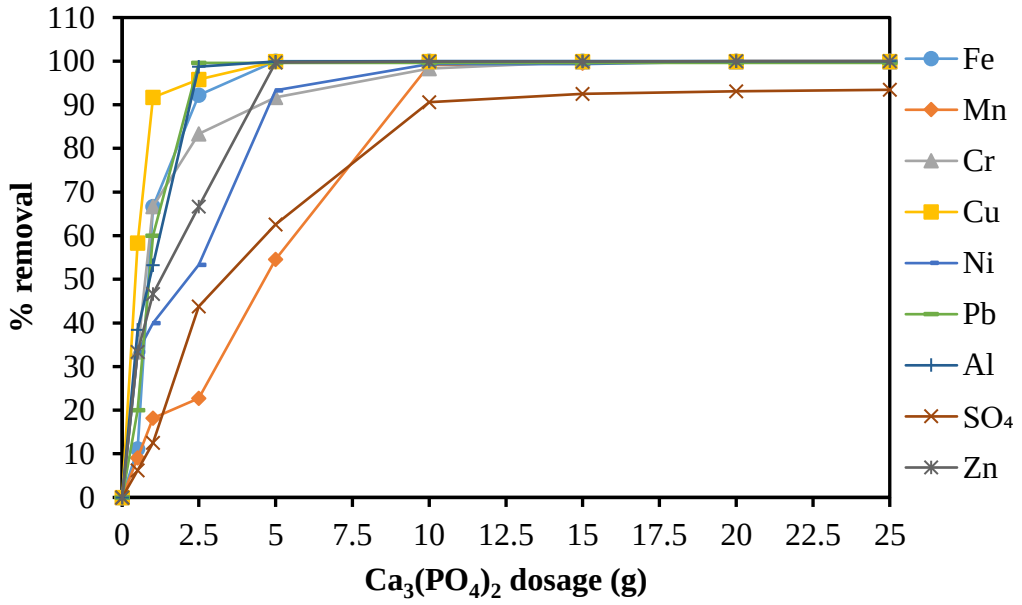

Figure 4: Variation in the percentage removals of the chemical species contained in acid mine drainage (AMD) with increasing $Ca_3(PO_4)_2$ dosages (AMD volume 1000 mL, 90 min contact time at 250 rpm mixing speed, and ambient temperature).

Figure 4 presents the results for the percentage removals of Fe, Mn, Cr, Cu, Ni, Pb, Al, SO_4, and Zn with increasing $Ca_3(PO_4)_2$ dosage. As was expected, there was an increase in the percentage removal of these contaminants with increasing $Ca_3(PO_4)_2$ dosage. Specifically, even at 1 g L^{-1} dosage Fe (66.7%), Cr (66.7%), Cu (91.7%), Pb (60.0%), Al (53.2%), and Zn (46.7%) concentrations were reduced to a large extent, while with increasing dosages the percentages

366 removals further improved. Specifically, at 5 g L^{-1} dosage Al (~100%), Cr (≥91.7%), Cu
367 (≥99.9%), Fe (~100%), Ni (93.3%) and Zn (≥99.7%) were grossly removed, while at dosage
368 10 g L^{-1} the removal percentages further improve (e.g., ≥99.8% for Cr, 99.1% for Mn, ≥99.3%
369 for Ni, 90.6% for SO_4, and ≥99.9% for Zn). Thereafter, trivial fluctuations were observed for
370 majority of the examined contaminants, apart from Ni which percentage removal reaches its
371 optimum at 15 g L^{-1} (≥99.3%) and SO_4 which reaches its maximum at the 25 g L^{-1} (93.4%).
372 For practical applications, the reagent dosage, in this case $Ca_3(PO_4)_2$, should be as low as
373 possible. Therefore, results suggest that the $Ca_3(PO_4)_2$ dosage should be at least 10 g L^{-1}, where
374 percentage removals are very high to optimum but not at the expense of $Ca_3(PO_4)_2$ mass.
375 Regarding the SO_4 content, this was not fully removed even at the higher examined dosage,
376 whereas there is a trade off in SO_4 removal and $Ca_3(PO_4)_2$ dosage, since after the 10 g L^{-1}
377 dosage, only small increases in the percentage removals of sulphate were observed. Therefore,
378 it appears that the 10 g L^{-1} is the optimum dosage for both metals and SO_4 removal.

379 **3.3 Treatment of AMD at optimum conditions**

380 After the optimum conditions for contact time and $Ca_3(PO_4)_2$ dosage were identified, the AMD
381 was thence treated under these conditions. These conditions were also examined in the
382 optimization studies for $Ca_3(PO_4)_2$ dosage (90 min contact time and 10 g L^{-1} dosage), however,
383 they are reported in more detail here as well. The physicochemical properties of the raw and
384 the $Ca_3(PO_4)_2$ treated AMD are reported in **Table 2**.

385 **Table 2:** The physicochemical properties of the concentrated AMD before and after treatment
386 with the synthesized $Ca_3(PO_4)_2$ at optimum conditions, i.e., 90 min contact time at 250 rpm, 10
387 g L^{-1} $Ca_3(PO_4)_2$ dosage, and room temperature.

Parameter	Units	Before treatment	After treatment	Percentage removal
pH	-	1.8	11.45	-
Acidity	mg L^{-1} $CaCO_3$	14950	0	-
EC	mS m^{-1}	2000	988	50.6%
Fe	mg L^{-1}	1800	0.02	~99.99%
Al	mg L^{-1}	500	0.01	~99.99%
Mn	mg L^{-1}	98	0.05	99.95%
SO_4	mg L^{-1}	11,986	1,128	90.59%
Ca	mg L^{-1}	500	659	-31.80%
Mg	mg L^{-1}	495	0.34	99.93%
Ni	mg L^{-1}	1.3	<0.087	>93.3%
Cr	mg L^{-1}	0.06	<0.001	>98.33%
Cu	mg L^{-1}	0.56	<0.001	>99.82%
Pb	mg L^{-1}	0.12	<0.01	>91.67%
Zn	mg L^{-1}	11	<0.03	>99.73%
P	mg L^{-1}	1.1	<0.001	>99.91%

As mentioned above, high-strength AMD (Strosnider and Nairn, 2010) was used in this work, which was highly acidic (pH 1.8). Specifically, according to Nordstrom et al. (2015) mine drainage could be acidic, neutral, and alkaline, and this is basically attributed to the pH, since the drainage is acidic (AMD) when the pH is ≤ 6, neutral when the pH is between 6 to 9 is and alkaline when the pH is >9. Apart from the pH the acidity of the collected mine water was very high, i.e., 14950 mg L^{-1} $CaCO_3$, hence denoting that this effluent is AMD and requires notable buffering capacity to offset the acidity. Furthermore, due to its very low pH the metals and SO_4

concentrations were particularly high, which is typical for AMD with high acidity (Bologo et al., 2012, Nordstrom et al., 2015, Mogashane et al., 2022). However, even though high-strength AMD (Strosnider and Nairn, 2010) was used herein, it was identified that the low-value P material (Masindi and Foteinis, 2021) synthesized and recovered from the MWW dewatering sludge stream, i.e., $Ca_3(PO_4)_2$, can provide an alternative solution for the effective management of AMD. This also suggest the potential of $Ca_3(PO_4)_2$ for the treatment of less concentrated AMD and, most likely, for the treatment of neutral drainage. Specifically, $Ca_3(PO_4)_2$ treatment largely reduced the levels of the contaminants contained in AMD, suggesting that it is possible to valorize MWW through P recovery and then employ it for the treatment of another wastewater matrix, i.e., AMD. This MWW-AMD management process makes use of the combined effect between different contaminants contained in these wastewater matrices. Specifically, the treatment of MWW with $Ca(OH)_2$ greatly improves MWW's physicochemical quality with the nutrients and microbial load being greatly reduced/eliminated (**Table 1**). Thereafter, the recovered $Ca_3(PO_4)_2$ was used to effectively treat the AMD, with the contaminants of major concern being greatly removed (**Table 2**). In detail, the pH was observed to increase from 1.8 to 11.45, indicating that the alkalinity released from the $Ca_3(PO_4)_2$ matrix will be instrumental in metals and minerals precipitation. It was observed that Al and Fe were practically removed (~99.99%), while the percentage removal for Cr being ≥99.82%, ≥98.33% for Cu, ≥93.3% for Ni, 99.95% for Mn, 99.93% for Mg, ≥91.67% for Pb, and 99.73% for Zn. Furthermore, a large reduction (90.59%) in the SO_4 content was also observed, while EC was also reduced by ≥50.6%.

Regarding the Ca level, this was not reduced but instead was increased by 31.8%, since Ca was released during $Ca_3(PO_4)_2$ dissolution, although it contributed to the attenuation of sulphate. As was the case with the $Ca(OH)_2$ treated MWW, the pH of the $Ca_3(PO_4)_2$ treated AMD was

high (≥11.45), suggesting that different pathways can be pursued for the correction of its pH (e.g., flue gas or air bubbling, or mixing raw AMD as to treat both the raw AMD and neutralise the pH of the $Ca_3(PO_4)_2$ treated effluent) or simply neutralise it the using low-cost and readily available acids such as sulfuric (H_2SO_4) or hydrochloric (HCl) acid. Finally, the high pH value suggest that the treated effluent will also be disinfected, to a large extent, as was the case with MWW (**Table 1**).

Therefore, results suggest that this indirect co-treatment method, which relies on the affinity of the contaminants contained in MWW and AMD, could be promising for the management of both matrices and particularly in the developing world setting where wastewater infrastructure is typically undeveloped or underdeveloped (Masindi et al., 2022b). More importantly, both treated effluents can provide an alternative source of water, e.g., for irrigation or even for groundwater recharge, provided that further treatment is pursued, and therefore address, at least partly, water availability concerns in water-scarce countries such as South Africa. Overall, this indirect MWW-AMD co-treatment method appears to be promising for the effective management of both effluents, while, at the same time, it could open new avenues for water reclamation, and therefore also promote UN's SDGs. To further support the aforementioned results for the aqueous matrices under study, detailed characterizations of the solid materials that were used and produced during MWW (i.e., $Ca(OH)_2$ and $Ca_3(PO_4)_2$) and AMD (resultant sludge) treatment were also carried out. It should be noted that the procured $Ca(OH)_2$, as well as the synthesized $Ca_3(PO_4)_2$ have been also characterised elsewhere (Masindi and Foteinis, 2021).

3.4 Solid materials characterization

This section provides insight on the fate of chemical species contained in MWW and AMD post their interaction with the $Ca(OH)_2$ and the synthesized $Ca_3(PO_4)_2$, respectively. For this reason, both the $Ca(OH)_2$ and the $Ca_3(PO_4)_2$ matrices were characterized, along with the resultant sludge (the sludge that is produced from the interaction of AMD with $Ca_3(PO_4)_2$). By doing so, the results regarding the quality of the treated MWW and AMD are corroborated and verified.

3.4.1 Elemental composition using XRF

First, the elemental compositions of $Ca(OH)_2$, $Ca_3(PO_4)_2$, and the resultant sludge were identified by means of XRF and results are shown in **Table 3.**

Table 3: The elemental composition of $Ca(OH)_2$, $Ca_3(PO_4)_2$, and the resultant sludge as measured by XRF.

	XRF results (wt. %)		
Oxides	$Ca(OH)_2$	$Ca_3(PO_4)_2$	Resultant sludge
SiO_2	2.78	3.11	1.89
Al_2O_3	0.60	0.64	2.21
MgO	1.09	1.68	2.22
Na_2O	0.15	0.14	0.21
P_2O_5	0.09	4.41	0.35
Fe_2O_3	0.29	0.35	23.82
K_2O	<0.01	<0.01	<0.01

CaO	71.35	62.11	37.80
TiO_2	0.02	0.02	0.01
V_2O_5	<0.01	<0.01	<0.01
Cr_2O_3	<0.01	<0.01	<0.01
MnO	0.01	0.00	0.24
NiO	<0.01	<0.01	<0.01
CuO	<0.01	<0.01	<0.01
ZrO_2	0.01	0.02	<0.01
SO_3	1.11	1.57	24.16
Nb_2O_5	<0.01	0.01	<0.01
CO_3O_4	<0.01	<0.01	0.02
ZnO	<0.01	<0.01	0.02
SrO	0.29	0.23	0.12
Y_2O_3	<0.01	<0.01	0.01
LOI	22.17	23.95	6.89
Total	**99.95**	**98.25**	**99.97**

As shown in **Table 3**, $Ca(OH)_2$ comprised Ca as its major element along with traces of Si and Mg, which are impurities typically contained in the parent material (limestone). The loss of ignition (LOI) was also observed to be high. This could be mainly traced back to water, since this material is hydrated, and to a lesser extent to volatile compounds, organic matter, and carbonates. The presence of Ca aids the removal of phosphate from municipal wastewater as $Ca_3(PO_4)_2$, while the added alkalinity also aids the removal of ammonia as nitrogen gas (Masindi and Foteinis, 2021). Regarding the $Ca_3(PO_4)_2$ matrix, this was enriched with P, Ca, Si, and Mg (**Table 3**). The presence of Si and Mg suggest the co-precipitation of these chemical

460 species along with P from MWW and that these elements will exists as impurities in the
461 $Ca_3(PO_4)_2$ matrix. However, Mg and Si are not considered contaminants, whereas their
462 existence can be beneficial through alkalinity addition. Finally, the resultant sludge was found
463 to contain elevated levels of Ca, Fe, Al, Mn, Mg, and S, along with traces of Al, Si, Mg, and
464 Mn (**Table 3**). These elements were also present in the raw AMD matrix (**Table 2**), which
465 implies their precipitation from AMD to the resultant sludge. Therefore, result suggest that the
466 resultant sludge is a sink for the predominant chemical species contained in AMD, which
467 highlights the efficiency of the $Ca_3(PO_4)_2$ treatment process.

468 **3.4.2 Map sum spectrums**

469 To corroborate the XRF results, the SEM-EDS spectrums for $Ca(OH)_2$, $Ca_3(PO_4)_2$, and the
470 resultant sludge were also obtained. The corresponding spectrums along with the estimated
471 surface elemental compositions are shown in **Figure 5**.

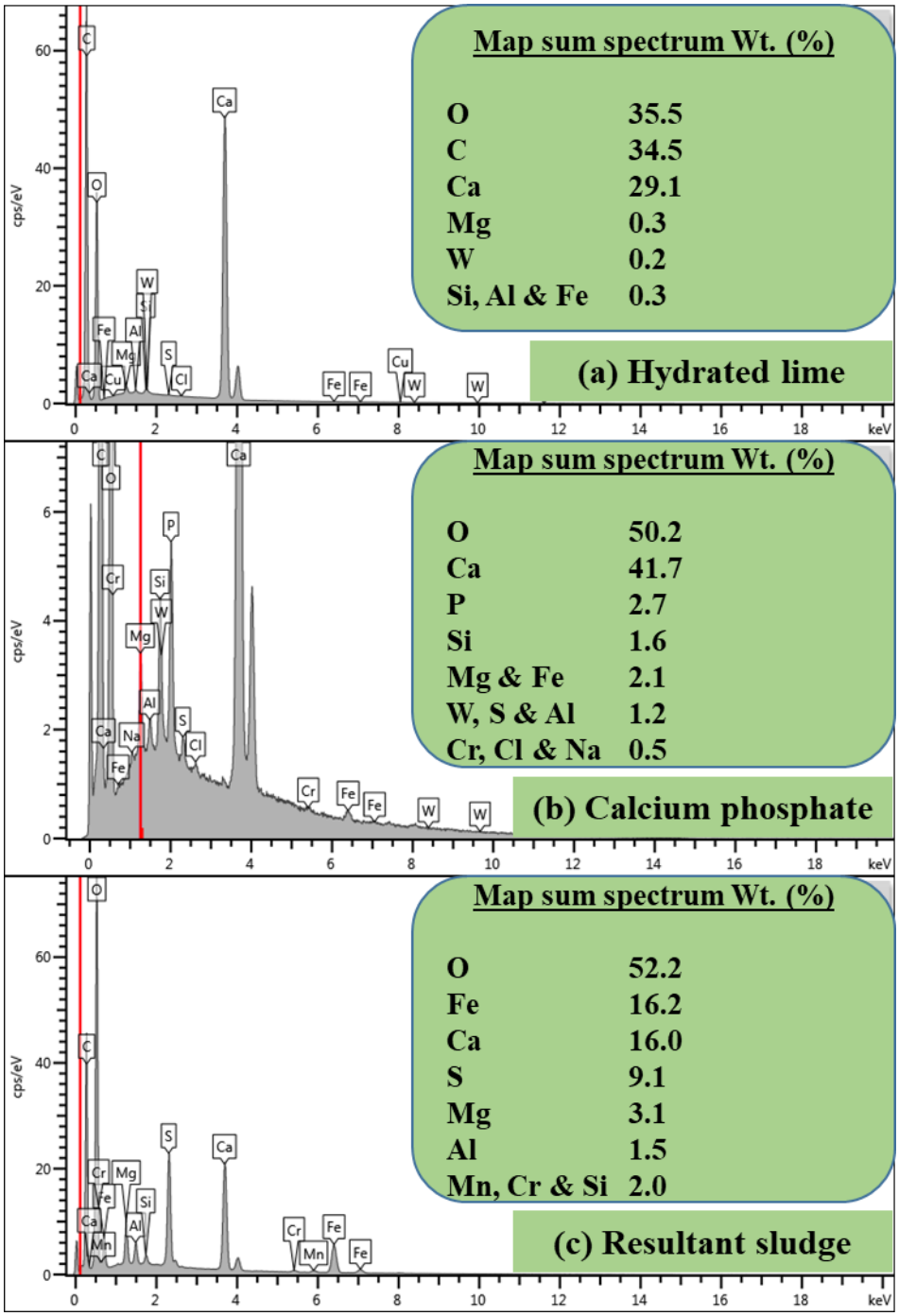

472

473 **Figure 5:** Elemental composition of (a) $Ca(OH)_2$, (b) $Ca_3(PO_4)_2$, and (c) resultant sludge using

474 the SEM-EDS spectrums.

475 Specifically, $Ca(OH)_2$ was found to include of Ca, C, and O as major elements, along with

476 traces of Mg, Fe, Si, Al, and W. The presence of O is traced back to the fact that $Ca(OH)_2$ is a

hydroxide, while C can be traced back to the coating (fine carbon layers) that is was in the SEM measurements to improve the imaging of samples and not the material itself and therefore it is not considered here. The SEM-EDS results for $Ca_3(PO_4)_2$ also support the XRF results, since Ca, O, and P were identified, among others minors elements. Finally, the resultant sludge was rich in Fe, O, S, and Ca, and traces of Mg, Al, Mn, Cr, and Si (**Figure 5**). The interaction of calcium rich effluent with AMD will lead to the formation of numerous dissociates and minerals as shown below (Name and Sheridan, 2014):

$$MgSO_4 + Ca(OH)_2 + 2H_2O \rightarrow CaSO_4.2H_2O + Mg(OH)_2 \quad (1)$$

$$CaO + H_2O \rightarrow Ca(OH)_2 \quad (2)$$

$$Ca(OH)_2 \rightarrow Ca^{2+} + OH^- \quad (3)$$

$$Fe^{m+} + MOH^- \rightarrow Fe(OH)_m \quad (4)$$

$$Ca^{2+} + SO_4^{2-} + 2H_2O \rightarrow CaSO_4.2H_2O \quad (5)$$

In essence, base metals present in the matrices of calcium phosphate, i.e., Ca^{2+}, induce an increase in pH thus leading to the precipitation of metals as hydroxide (Eq. 6).

$$M^{n+} + nOH^- \rightarrow M(OH)_n \downarrow \quad (6)$$

Dissolution and dissociation of base metals, Ca^{2+} and Mg^{2+}, is summarised in Eq. (7) – (8) (Masindi et al., 2017).

$$MgO + H_2O \rightarrow Mg^{2+} + 2OH^- \quad (7)$$

$$CaO + H_2O \rightarrow Ca^{2+} + 2OH^- \quad (8)$$

As expected, this induces an increase in the pH thus fostering neucleation, crystallization, and flocs which settle down as precipitants. The obtained results are congruent with the XRF, XRD, FTIR, and SEM mapping results.

Overall, both the XRF and SEM-EDS results highlight that the concentration of the recovered P is low and therefore the synthesized $Ca_3(PO_4)_2$ can be considered as a low-value P material

with limited viable pathways for valorisation. Finally, the EDS results also corroborate the XRF results and highlight that the resultant sludge is a sink for the chemical species contained in the AMD. This highlights the potential of $Ca_3(PO_4)_2$ for AMD treatment.

3.4.3 Morphological properties

The morphological properties and microstructural characteristics of $Ca(OH)_2$, $Ca_3(PO_4)_2$, and the resultant sludge are shown in **Figure 6**. To attain high quality imagery, with practically no distortion**,** HR-FE-FIB-SEM was employed.

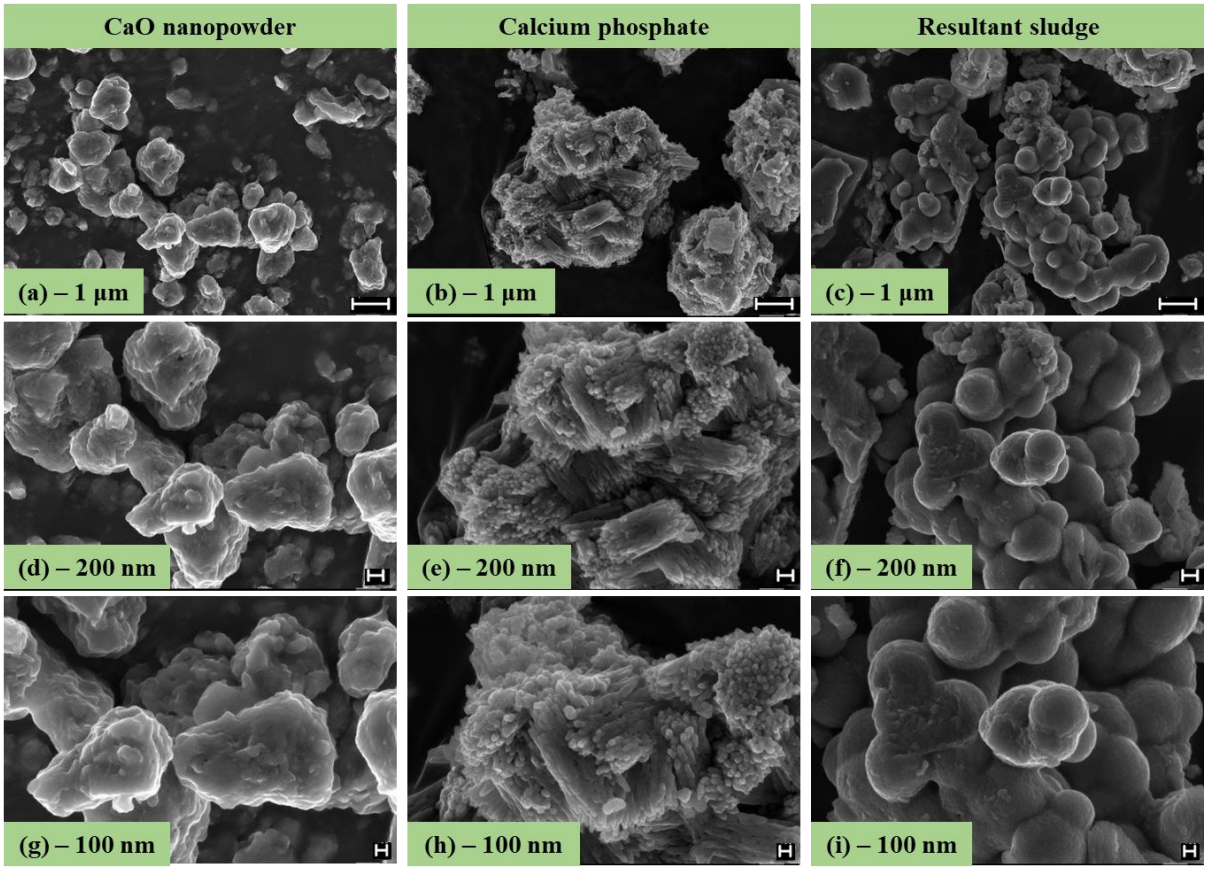

Figure 6: The HR-FE-FIB-SEM imagery showing the microstructural and morphological characteristics of $Ca(OH)_2$, $Ca_3(PO_4)_2$, and the resultant sludge at a-c) 1 µm, d-f) 200 nm, and g-i) 100 nm magnification.

In all examined samples, the morphological characteristics were observed to remain similar regardless of the magnification used. Furthermore, $Ca(OH)_2$ was found to comprise rectangular scales lumped together, whereas $Ca_3(PO_4)_2$ comprised rod-like structures lumped together. On the other hand, the produced sludge comprised spherical particles, which suggest the presence of Fe, connected to each other on a dendritic fashion (**Figure 6**). Therefore, results suggest the transformation of the $Ca_3(PO_4)_2$ to a new material (resultant sludge) which is rich in Fe, one of AMD's main contaminants.

3.4.4 Elemental distribution mapping using EDS

To further corroborate the XRF and the SEM-EDS results regarding the elemental compositions of the examined solid samples, elemental distribution mapping was also employed using the FE-SEM instrument with EDS capabilities. Results are shown in **Figure 7-9**.

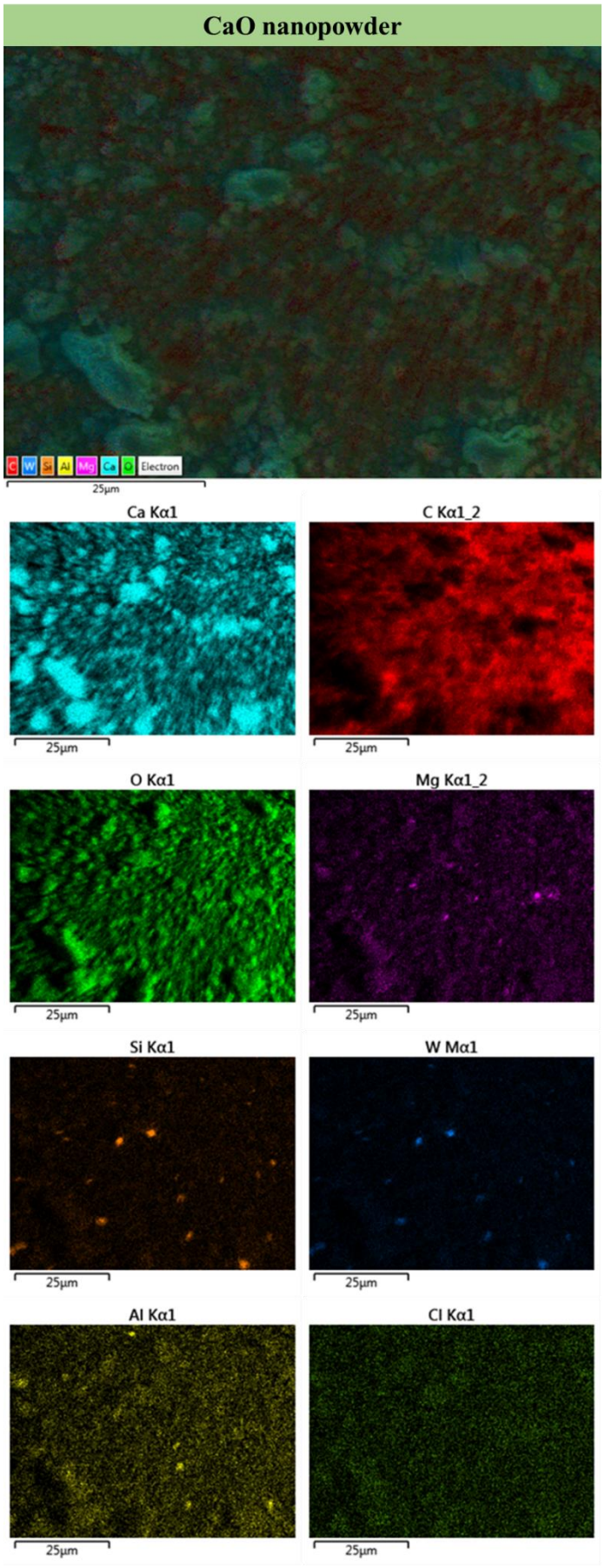
CaO nanopowder
C W Si Al Mg Ca O Electron
25µm
Ca Kα1
25µm
C Kα1_2
25µm
O Kα1
25µm
Mg Kα1_2
25µm
Si Kα1
25µm
W Mα1
25µm
Al Kα1
25µm
Cl Kα1
25µm

524

Figure 7: The SEM-EDS imagery and elemental maps of $Ca(OH)_2$.

As shown in **Figure 7,** $Ca(OH)_2$ comprised Ca, O, and C as dominant elements. Fair dispersion of other elements, i.e., Mg, Si, W, Al and Cl, was also observed.

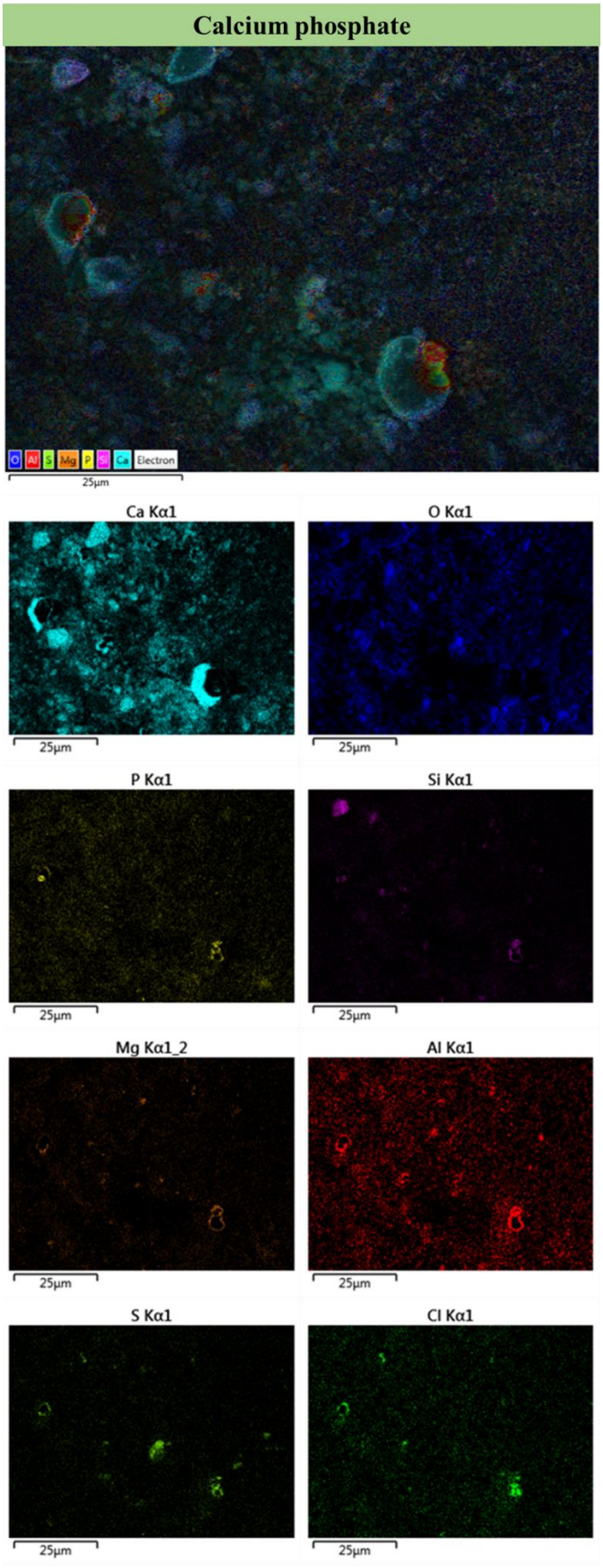
Calcium phosphate
O Al S Mg P Cl Ca Electron
25µm
Ca Kα1
25µm
O Kα1
25µm
P Kα1
25µm
Si Kα1
25µm
Mg Kα1_2
25µm
Al Kα1
25µm
S Kα1
25µm
Cl Kα1
25µm

528

Figure 8: The SEM-EDS imagery and elemental maps of $Ca_3(PO_4)_2$.

For $Ca_3(PO_4)_2$ (**Figure 8**), its main elements include Ca, O, and P, along with dispersed traces of Mg, Al, Si, S, and Cl. The presence of Ca, O and P denotes the formation of $Ca_3(PO_4)_2$.

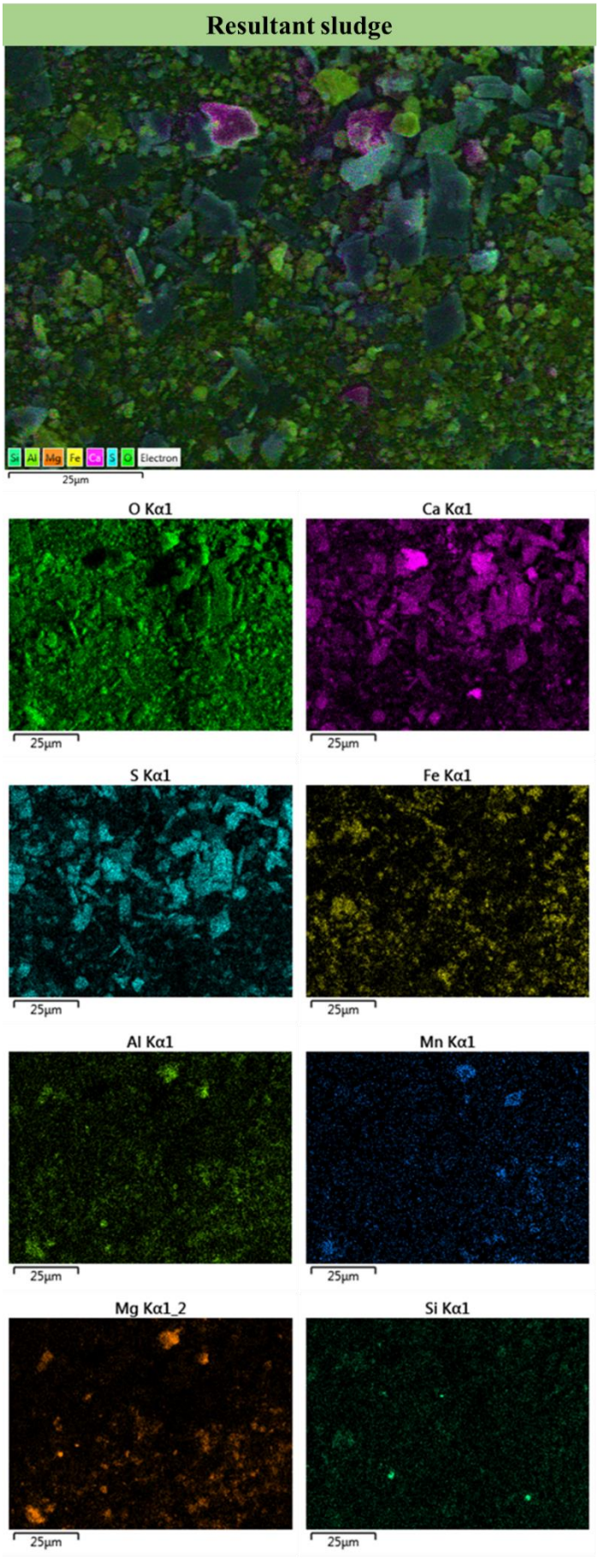
Resultant sludge
Si Al Mg Fe Ca S O Electron
25μm
O Kα1
25μm
Ca Kα1
25μm
S Kα1
25μm
Fe Kα1
25μm
Al Kα1
25μm
Mn Kα1
25μm
Mg Kα1_2
25μm
Si Kα1
25μm

532

Figure 9: The SEM-EDS imagery and elemental maps of the resultant sludge.

Finally, the resultant sludge comprised O, Ca, S and Fe as predominant elements, which were evenly distributed across the surface, while traces of other elements, such as Mn, Al, Mg and Si, were also identified (**Figure 9**). The presence of Ca, O, and S in the resultant sludge suggest the formation of gypsum, whilst the presence of Fe and O suggest the formation of Fe-hydroxides. The results of the elemental distribution mapping are in accordance with the results of the map sum spectrums.

3.4.5 Mineralogical properties

The mineralogical compositions of the examined solid samples were identified using XRD and results are shown in **Figure 10**.

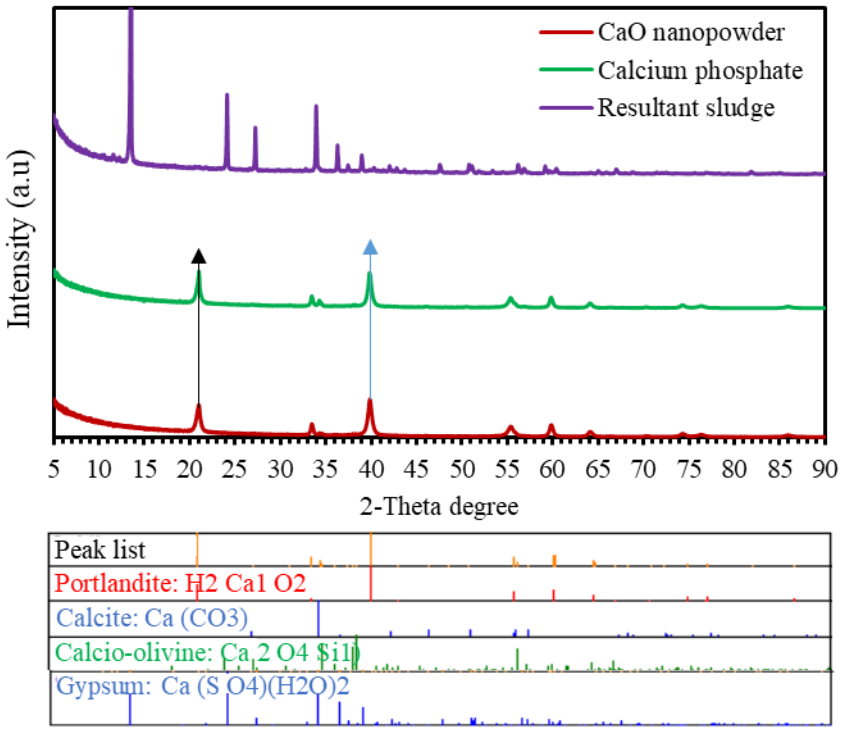

Figure 10: Mineralogical composition of $Ca(OH)_2$, $Ca_3(PO_4)_2$, and the resultant sludge.

As shown in **Figure 10**, the crystal phases of Ca(OH)2, $Ca_3(PO_4)_2$, and of the resultant sludge were identified. Specifically, $Ca(OH)_2$ comprised portlandite, calcite, and calico-olivine, which correspond to the Ca, O, and Si elements that were identified in the XRF and EDS analyses. Similarly, $Ca_3(PO_4)_2$ was predominated by portlandite, as the hydrated form of calcium. This is the crystalline phase hence denoting that the other elements detected using XRF and SEM-EDS are amorphous in nature. However, after $Ca_3(PO_4)_2$ contacts AMD new mineral phases were identified in the resultant sludge and primarily gypsum (due to the interaction of SO_4 with Ca). Finally, the noisy signal in the spectrogram of the resultant sludge denotes the presence of amorphous phases in its matrix (**Figure 10**).

3.4.6 Functional groups

Finally, the FTIR spectrums of the solid samples were also identified, along with their functional groups and wavenumbers (cm^{-1}). Results are shown in **Figure 11**.

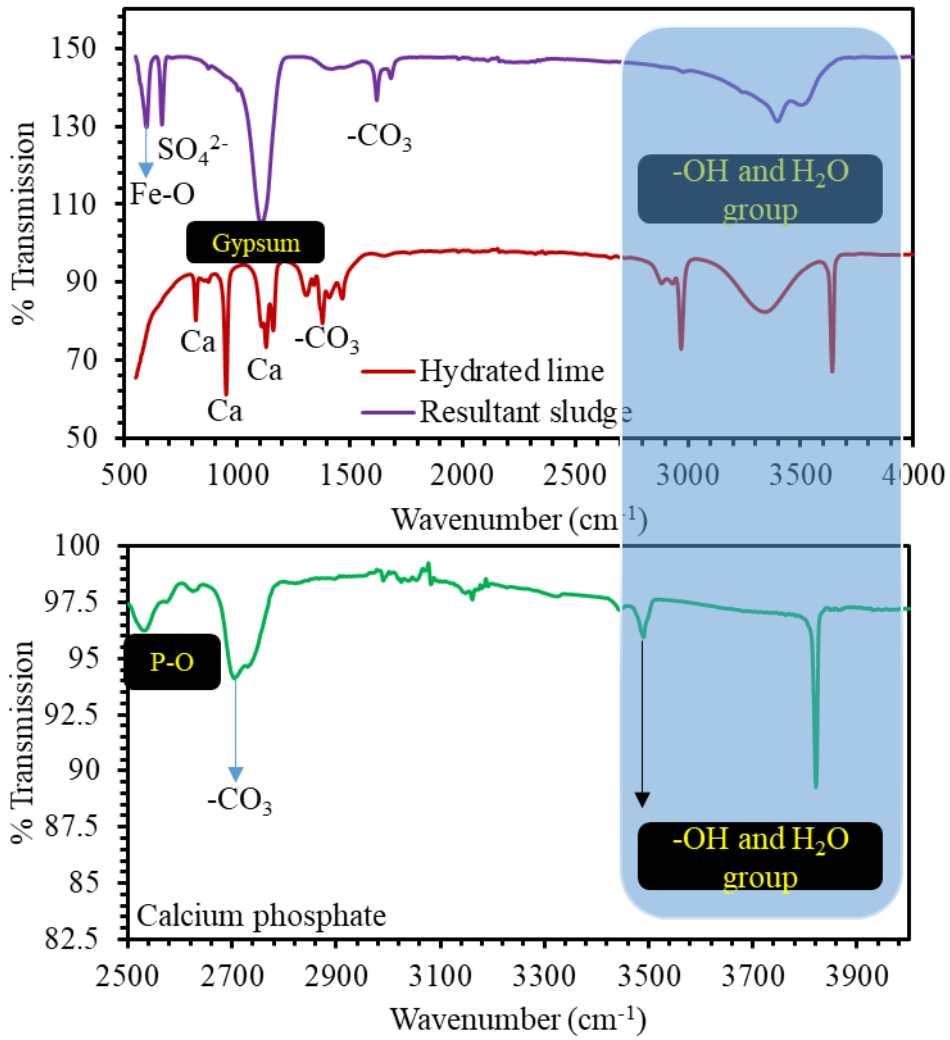

557

558 **Figure 11:** The FTIR spectrum of $Ca(OH)_2$, $Ca_3(PO_4)_2$, and of the resultant sludge along with
559 the identified functional groups.

560 As shown in **Figure 11**, the functional groups of $Ca(OH)_2$ comprised the carbonates duplex
561 (1500), hydroxyl groups from water (3000 and 3700 cm^{-1}), and Ca (800, 1000, and 1200 cm^{-1})
562 (Masindi and Foteinis, 2021). These elements will contribute to the removal of phosphates
563 from raw MWW and towards the synthesis of $Ca_3(PO_4)_2$. Furthermore, the availability of water
564 (H_2O and -OH group) confirms that this material is hydrated. The functional groups of
565 $Ca_3(PO_4)_2$ include P-O (2600 cm^{-1}), CO_3 (2700 cm^{-1}), and OH^- (3800 cm^{-1}), hence confirming

566 the formation of a phosphate-based mineral (Masindi and Foteinis, 2021). Finally, the resultant
567 sludge comprised Fe-O (550 cm^{-1}), SO_4 (700 cm^{-1}), gypsum (1200 cm^{-1}), CO_3 (1600 cm^{-1}), and
568 OH^- (3600 cm^{-1}). The presence of Fe and OH groups denotes the formation of Fe-hydroxide,
569 whilst the presence of gypsum confirms the sink of SO_4 from AMD and Ca from $Ca_3(PO_4)_2$
570 into the resultant sludge (Tabelin et al., 2017, Masindi and Foteinis, 2021, Masindi et al.,
571 2022b).Therefore, the FTIR results corroborate the XRF, XRD, and EDS/SEM results.

572 Overall, it appears that the use of $Ca_3(PO_4)_2$, which has been recovered from MWW, can act
573 as an innovative avenue for the treatment of AMD. Furthermore, regarding the produced sludge
574 from the treatment of AMD, many contaminants were identified along with valuable minerals
575 which precipitated from AMD to the produced sludge. This suggest that opportunities for their
576 recovery from the AMD sludge and for water reclamation might exists. Furthermore, to
577 sustainably upscale this promising co-treatment technology a full techno-economic analysis
578 (TEA) and life cycle assessment (LCA) are also required. All the above will be studied in future
579 works of our group. Overall, with this indirect co-treatment method the effective co-
580 management of both MWW and AMD can be achieved, while water could possibly be
581 reclaimed. This is of particularly importance for South Africa and other countries and areas
582 that are affected by water scarcity.

583 **4 Conclusions and recommendations**

584 The synthesis of calcium phosphate ($Ca_3(PO_4)_2$) from municipal wastewater (MWW) and its
585 novel application for the treatment of acid mine drainage (AMD), collected from an active coal
586 mine in South Africa, was successfully explored. Specifically, MWW was first reacted with
587 calcium hydroxide ($Ca(OH)_2$) towards the synthesis of $Ca_3(PO_4)_2$. In this process, MWW was
588 also treated, to a large extend, suggesting that with further treatment, i.e., using a treatment

train approach, water could also be reclaimed. Through this process, a low-value phosphorous (P) material, due to MWW's low P concentration, was synthesized and recovered, i.e., $Ca_3(PO_4)_2$, from municipal wastewater. However, here, this a low-value P material was found to be particularly promising for the treatment of concentrated AMD. The optimum conditions for AMD treatment with the synthesized $Ca_3(PO_4)_2$ were identified as 10 g $Ca_3(PO_4)_2$ of dosage in 1L of AMD and 90 minutes of contact time (mixing). With this indirect MWW-AMD co-treatment process, AMD was effectively treated, since the main contaminants that are typically embedded in its matrix, i.e., Fe, Mn, Cr, Cu, Ni, Pb, Al, SO_4, and Zn, were practically removed. Furthermore, the SO_4 content was also greatly reduce (90.6%). To identify the fate of the contaminants from both wastewater matrices, i.e., MWW and AMD, post their treatment, the produced solid material (sludge) along with $Ca(OH)_2$ and $Ca_3(PO_4)_2$ were also characterised. The results for solid samples characterization corroborated the results of the treated MWW and AMD matrices.

Overall, results suggested that this indirect co-management method can be an effective solution for the treatment of the ever-increasing quantities of both MWW and AMD, particularly in the developing world setting where their treatment remains problematic. Furthermore, this treatment method could play a large role in minimizing the ecological impact from the release of untreated MWW and AMD and at the same time the treated effluents could be used for water reclamation. This is of major importance in water scarce countries, such as South Africa. Specifically, with further treatment water from these effluents could be used for irrigation or even for groundwater recharge or for drinking water purposes, thus also promoting United Nations' (UN) Sustainable Development Goals (SDGs).

Acknowledgement

612 The authors of this manuscript would like to convey their sincere and profound gratitude to the
613 University of South Africa, the University of Venda, Council for Scientific and Industrial
614 Research, University of Pretoria, and Magalies Water for extending their facilities and funding
615 towards the accomplishment of this project. The mining houses and municipal wastewater
616 facilities who granted researchers in this study permission to collect the effluents are also
617 acknowledged.

References

Adler, P. R. & Sibrell, P. L. 2003. Sequestration of Phosphorus by Acid Mine Drainage Floc. Journal of environmental quality, 32**,** 1122-1129.

Amann, A., Zoboli, O., Krampe, J., Rechberger, H., Zessner, M. & Egle, L. 2018. Environmental impacts of phosphorus recovery from municipal wastewater. Resources, Conservation and Recycling, 130**,** 127-139.

Arola, K., Van Der Bruggen, B., Mänttäri, M. & Kallioinen, M. 2019. Treatment options for nanofiltration and reverse osmosis concentrates from municipal wastewater treatment: A review. Critical Reviews in Environmental Science and Technology, 49**,** 2049-2116.

Baker, B. J. & Banfield, J. F. 2003. Microbial communities in acid mine drainage. FEMS Microbiology Ecology, 44**,** 139-152.

Barthen, R., Sulonen, M. L. K., Peräniemi, S., Jain, R. & Lakaniemi, A.-M. 2022. Removal and recovery of metal ions from acidic multi-metal mine water using waste digested activated sludge as biosorbent. Hydrometallurgy, 207**,** 105770.

Bologo, V., Maree, J. P. & Carlsson, F. 2012. Application of magnesium hydroxide and barium hydroxide for the removal of metals and sulphate from mine water. Water SA, 38**,** 23-28.

Bouwer, H. 2000. Integrated water management: emerging issues and challenges. Agricultural Water Management, 45**,** 217-228.

Bunce, J. T., Ndam, E., Ofiteru, I. D., Moore, A. & Graham, D. W. 2018. A Review of Phosphorus Removal Technologies and Their Applicability to Small-Scale Domestic Wastewater Treatment Systems. Frontiers in Environmental Science, 6.

Calli, B., Mertoglu, B. & Inanc, B. 2005. Landfill leachate management in Istanbul: applications and alternatives. Chemosphere, 59**,** 819-829.

642 Dunets, C. S. & Zheng, Y. 2014. Removal of phosphate from greenhouse wastewater using
643 hydrated lime. Environmental Technology, 35**,** 2852-2862.
644 Greenberg, A. E., Clesceri, L. S. & Eaton, A. D. 2010. Standard Methods for the Examination
645 of Water and Wastewater.
646 Hughes, T. A. & Gray, N. F. 2013a. Co-treatment of acid mine drainage with municipal
647 wastewater: Performance evaluation. Environmental Science and Pollution Research,
648 20**,** 7863-7877.
649 Hughes, T. A. & Gray, N. F. 2013b. Removal of Metals and Acidity from Acid Mine Drainage
650 Using Municipal Wastewater and Activated Sludge. Mine Water and the Environment,
651 32**,** 170-184.
652 Kefeni, K. K., Msagati, T. a. M. & Mamba, B. B. 2017. Acid mine drainage: Prevention,
653 treatment options, and resource recovery: A review. Journal of Cleaner Production, 151**,**
654 475-493.
655 Kim, E. J., Kim, H. & Lee, E. 2021. Influence of Ammonia Stripping Parameters on the
656 Efficiency and Mass Transfer Rate of Ammonia Removal. Applied Sciences, 11**,** 441.
657 Maree, J. P., Mujuru, M., Bologo, V., Daniels, N. & Mpholoane, D. 2013. Neutralisation
658 treatment of AMD at affordable cost. Water SA, 39**,** 245-250.
659 Masindi, V., Fosso-Kankeu, E., Mamakoa, E., Nkambule, T. T. I., Mamba, B. B., Naushad, M.
660 & Pandey, S. 2022a. Emerging remediation potentiality of struvite developed from
661 municipal wastewater for the treatment of acid mine drainage. Environmental Research,
662 210**,** 112944.
663 Masindi, V. & Foteinis, S. 2021. Recovery of phosphate from real municipal wastewater and
664 its application for the production of phosphoric acid. Journal of Environmental
665 Chemical Engineering, 9**,** 106625.

Masindi, V., Foteinis, S. & Chatzisymeon, E. 2022b. Co-treatment of acid mine drainage and municipal wastewater effluents: Emphasis on the fate and partitioning of chemical contaminants. Journal of Hazardous Materials, 421**,** 126677.

Masindi, V., Foteinis, S., Renforth, P., Ndiritu, J., Maree, J. P., Tekere, M. & Chatzisymeon, E. 2022c. Challenges and avenues for acid mine drainage treatment, beneficiation, and valorisation in circular economy: A review. Ecological Engineering, 183**,** 106740.

Masindi, V., Gitari, M. W., Tutu, H. & Debeer, M. 2017. Synthesis of cryptocrystalline magnesite–bentonite clay composite and its application for neutralization and attenuation of inorganic contaminants in acidic and metalliferous mine drainage. Journal of Water Process Engineering, 15**,** 2-17.

Masindi, V., Madzivire, G. & Tekere, M. 2018a. Reclamation of water and the synthesis of gypsum and limestone from acid mine drainage treatment process using a combination of pre-treated magnesite nanosheets, lime, and CO_2 bubbling. Water Resources and Industry, 20**,** 1-14.

Masindi, V., Ndiritu, J. G. & Maree, J. P. 2018b. Fractional and step-wise recovery of chemical species from acid mine drainage using calcined cryptocrystalline magnesite nano-sheets: An experimental and geochemical modelling approach. Journal of Environmental Chemical Engineering, 6**,** 1634-1650.

Masindi, V., Osman, M. S., Mbhele, R. N. & Rikhotso, R. 2018c. Fate of pollutants post treatment of acid mine drainage with basic oxygen furnace slag: Validation of experimental results with a geochemical model. Journal of Cleaner Production, 172**,** 2899-2909.

688 Masindi, V., Shabalala, A. & Foteinis, S. 2022d. Passive co-treatment of phosphorus-depleted
689 municipal wastewater with acid mine drainage: Towards sustainable wastewater
690 management systems. Journal of Environmental Management, 324**,** 116399.
691 Mavhungu, A., Foteinis, S., Mbaya, R., Masindi, V., Kortidis, I., Mpenyana-Monyatsi, L. &
692 Chatzisymeon, E. 2020. Environmental sustainability of municipal wastewater
693 treatment through struvite precipitation: Influence of operational parameters. Journal of
694 Cleaner Production**,** 124856.
695 Mogashane, T. M., Maree, J. P., Letjiane, L., Masindi, V., Modibane, K. D., Mujuru, M. &
696 Mphahlele-Makgwane, M. M. 2022. Recovery of Drinking Water and Nanosized Fe 2
697 O 3 Pigment from Iron Rich Acid Mine Water. Application of Nanotechnology in
698 Mining Processes.
699 Naidu, G., Ryu, S., Thiruvenkatachari, R., Choi, Y., Jeong, S. & Vigneswaran, S. 2019. A
700 critical review on remediation, reuse, and resource recovery from acid mine drainage.
701 Environmental Pollution, 247**,** 1110-1124.
702 Name, T. & Sheridan, C. 2014. Remediation of acid mine drainage using metallurgical slags.
703 Minerals Engineering, 64**,** 15-22.
704 Neculita, C. M. & Rosa, E. 2019. A review of the implications and challenges of manganese
705 removal from mine drainage. Chemosphere, 214**,** 491-510.
706 Nordstrom, D. K., Blowes, D. W. & Ptacek, C. J. 2015. Hydrogeochemistry and microbiology
707 of mine drainage: An update. Applied Geochemistry, 57**,** 3-16.
708 O'farrell, T. P., Frauson, F. P., Cassel, A. F. & Bishop, D. F. 1972. Nitrogen Removal by
709 Ammonia Stripping. Journal (Water Pollution Control Federation), 44**,** 1527-1535.

710 Oehmen, A., Lemos, P. C., Carvalho, G., Yuan, Z., Keller, J., Blackall, L. L. & Reis, M. a. M.
711 2007. Advances in enhanced biological phosphorus removal: From micro to macro
712 scale. Water Research, 41**,** 2271-2300.
713 Park, I., Tabelin, C. B., Jeon, S., Li, X., Seno, K., Ito, M. & Hiroyoshi, N. 2019. A review of
714 recent strategies for acid mine drainage prevention and mine tailings recycling.
715 Chemosphere, 219**,** 588-606.
716 Petrie, B., Barden, R. & Kasprzyk-Hordern, B. 2015. A review on emerging contaminants in
717 wastewaters and the environment: Current knowledge, understudied areas and
718 recommendations for future monitoring. Water Research, 72**,** 3-27.
719 Qteishat, O., Myszograj, S. & Suchowska-Kisielewicz, M. 2011. Changes of wastewater
720 characteristic during transport in sewers. WSEAS Transactions on Environment and
721 Development, 7.
722 Rahman, A., Hasan, M., Meerburg, F., Jimenez, J., Miller, M., Bott, C., Al-Omari, A., Murthy,
723 S., Shaw, A., De Clippeleir, H. & Riffat, R. 2020. Moving forward with A-stage and
724 high-rate contact-stabilization for energy efficient water resource recovery facility:
725 Mechanisms, factors, practical approach, and guidelines. Journal of Water Process
726 Engineering, 36**,** 1-13.
727 Ruihua, L., Lin, Z., Tao, T. & Bo, L. 2011. Phosphorus removal performance of acid mine
728 drainage from wastewater. Journal of Hazardous Materials, 190**,** 669-676.
729 Sekhon, B. S. & Bhumbla, D. K. 2013. Phosphorus remediation by acid mine drainage floc and
730 its implications for phosphorus environmental indices. Journal of Soils and Sediments,
731 13**,** 336-343.
732 Sheoran, V., Sheoran, A. & Choudhary, R. P. 2011. Biogeochemistry of acid mine drainage
733 formation: A review. Mine Drainage and Related Problems**,** 119-154.

734 Simate, G. S. & Ndlovu, S. 2014. Acid mine drainage: Challenges and opportunities. Journal
735 of Environmental Chemical Engineering, 2**,** 1785-1803.
736 Soucek, D. J., Cherry, D. S. & Trent, G. C. 2000. Relative acute toxicity of acid mine drainage
737 water column and sediments to Daphnia magna in the Puckett's Creek watershed,
738 Virginia, USA. Archives of Environmental Contamination and Toxicology, 38**,** 305-
739 310.
740 Spellman, C. D., Tasker, T. L., Strosnider, W. H. J. & Goodwill, J. E. 2020. Abatement of
741 circumneutral mine drainage by Co-treatment with secondary municipal wastewater.
742 Journal of Environmental Management, 271**,** 110982.
743 Strosnider, W. H. & Nairn, R. W. 2010. Effective passive treatment of high-strength acid mine
744 drainage and raw municipal wastewater in Potosí, Bolivia using simple mutual
745 incubations and limestone. Journal of Geochemical Exploration, 105**,** 34-42.
746 Strosnider, W. H., Winfrey, B. K. & Nairn, R. W. 2011a. Alkalinity Generation in a Novel
747 Multi-stage High-strength Acid Mine Drainage and Municipal Wastewater Passive Co-
748 treatment System. Mine Water and the Environment, 30**,** 47-53.
749 Strosnider, W. H. J., Winfrey, B. K. & Nairn, R. W. 2011b. Novel passive Co-treatment of acid
750 mine drainage and municipal wastewater. Journal of Environmental Quality, 40**,** 206-
751 213.
752 Tabelin, C. B., Veerawattananun, S., Ito, M., Hiroyoshi, N. & Igarashi, T. 2017. Pyrite
753 oxidation in the presence of hematite and alumina: I. Batch leaching experiments and
754 kinetic modeling calculations. Science of The Total Environment, 580**,** 687-698.
755 The United Nations 2018. The Sustainable Development Goals Report. In: THE UNITED
756 NATIONS & DEPARTMENT OF ECONOMIC AND SOCIAL AFFAIRS. (eds.).

Tilbury, A., Deere, D., Rodriguez, C., Vorster, F., Fox, N., Marunczyn, M. & Piper, B. 2017. Validation of alkaline disinfection for recycled water schemes. Hydrometallurgy, 170**,** 82-89.

Tong, L., Fan, R., Yang, S., Zhang, Q. & Pan, Y. 2021. A technology review on treatment of acid mine drainage with bentonite–steel slag composite. SN Applied Sciences, 4**,** 10.

Un Habitat and Who 2021. Progress on wastewater treatment – Global status and acceleration needs for SDG indicator 6.3.1. Global status and acceleration needs for SDG indicator 6.3.1. Geneva: United Nations Human Settlements Programme (UN-Habitat) and World Health Organization (WHO).

United Nations. 2017. WWAP (United Nations World Water Assessment Programme). The United Nations World Water Development Report 2017. Wastewater: The Untapped Resource. Paris, UNESCO. UNESCO Publishing, 7, place de Fontenoy, 75352 Paris 07 SP France.

Vo, T.-D.-H., Le, V.-G., Nguyen, Q.-H., Pham, T.-T., Bui, T.-V., Dang, B.-T., Hoang, T.-T.-N., Son, N. T., Lin, K.-Y. A. & Bui, X.-T. 2022. Effects of storage conditions, pH and Mg:P ratio on the precipitation process for phosphate recovery. Case Studies in Chemical and Environmental Engineering, 5**,** 100188.

Weaver, D. M. & Ritchie, G. S. P. 1994. Phosphorus removal from piggery effluents of varying quality using lime and physico-chemical treatment methods. Environmental Pollution, 84**,** 237-244.

Wei, X., Rodak, C. M., Zhang, S., Han, Y. & Wolfe, F. A. 2016. Mine drainage generation and control options. Water Environment Research, 88**,** 1409-1432.

Wei, X., Viadero Jr, R. C. & Bhojappa, S. 2008. Phosphorus removal by acid mine drainage sludge from secondary effluents of municipal wastewater treatment plants. Water Research, 42**,** 3275-3284.

Yulianto, I., Moersidik, S. S. & Amanda, N. 2021. Comparative Phosphorus Removal Efficiency from Municipal Wastewater Using Acid Mine Drainage Sludge and Its H₂O₂ Activated form As Adsorbents. IOP Conference Series: Earth and Environmental Science, 721**,** 012010.

Zhao, Q., Han, H., Hou, B., Zhuang, H., Jia, S. & Fang, F. 2014. Nitrogen removal from coal gasification wastewater by activated carbon technologies combined with short-cut nitrogen removal process. Journal of Environmental Sciences, 26**,** 2231-2239.